Poster presented at the 18th Course: Nanostructured Carbon For Advanced Applications, A NATO Advanced Institute, Erice, Sicily, 19-31 July 2000

LOW - FIELD ELECTRON EMISSION FROM DIAMOND/PYROCARBON COMPOSITES

A. V. Karabutov[1], V. G. Ralchenko[1], S. K. Gordeev[2], P. I. Belobrov[3]

[1] General Physics Institute of Russian Academy of Sciences, Vavilova str. 38, Moscow 117942, Russia, e-mail: lx@ran.gpi.ru

[2] Central Research Institute of Materials, Paradnaya str. 8, St-Petersburg 191014, Russia

[3] Institute of Biophysics, Krasnoyarsk 660036, Russia

Abstract: *Field electron emission properties of diamond/pyrocarbon composites comprising diamond particles embedded into a sp^2-bonded carbon matrix are considered in dependence of their structure and composition. The emission at low fields >1 V/μm with "no activation/no hysteresis" current-voltage characteristics was reproducibly obtained on these materials. The diamond particle size was selected in the range of 5 nm - 5 μm, the carbon/diamond mass ratio being varied from 0 to 0.5. A Scanning Tunneling-Field Emission Microscopy was applied to study surface distribution of the field emission, work function, electrical conductivity, and morphology to understand the emission mechanisms. A similarity between this type of composite and CVD diamond films in structure and emission properties are observed. Mechanisms of the emission including field enhancement, band bending, and quantum well effects on the diamond/graphite interfaces are considered.*

1. Introduction

The phenomenon of field electron emission from diamond and a variety of carbon materials attracts a high interest of researchers. The effective emission was observed for CVD diamond films and single crystal diamond [1-8], diamond-like carbon films [9-11], nanotubes [12,13], and polymers [14]. In some cases the threshold fields are as low as 0.2-5 V/μm. However, the nature of the emission is not well understood. A common trend is that the low-field emission is observed mostly for carbon materials that contain at least a part of carbon with sp^2 bonds. It was found that the presence of graphitic phase [1,15-19] or defects [6] in diamond films improves the emission. Moreover, the emission was suggested to be associated with grain boundaries and diamond/graphite interfaces [1,3,8,15-17] that were confirmed experimentally by high-resolution emission mapping using STM devices [8,19-25].

Since the effective emission was reported also for carbon structures containing no sp^3 bonds such as nanotubes [12,13] and flake-like CVD graphite films [26,27], it follows that the presence of diamond phase that might exhibit negative electron affinity (NEA) [28-33] is not mandatory to provide a low-field emission. It is not clear, however, if the physical mechanisms of the emission are similar for the variety of the carbon materials with quite different structures (different bonding type).

Diamond/pyrocarbon composites [34,35], a new class of materials with low emission threshold fields [36-38] and easily controlled sp^2/sp^3 bonding ratio, are convenient objects to explore the question on a specific role, if any, of diamond component in the emission process. Here we present the experimental results and consider some models of low-field emission of the diamond/sp^2-bonded carbon composites with variable graphite (pyrocarbon) concentration and diamond grain size. The emission data reported by different authors for CVD diamond films are analyzed using the suggested models.

2. Experimental

The diamond/carbon composites contain diamond particles embedded into an sp^2-bonded carbon matrix grown by a pyrolytic process [34]. The graphitic matrix makes the composite conductive. The dimensions of diamond particles may span from a few nanometers to tens microns, and there is no graphitization of diamond during the pyrolytic process. The ultrafine diamond particles with average size of 5 nm produced by a detonation technique, and bigger grains produced by high pressure/high temperature technique, were used as the starting material in the composite fabrication. By filling the pores with pyrolytic carbon the mass ratio of sp^2-carbon-to-diamond (sp^2/sp^3 ratio) in the composites can be controlled (Fig.1). The composition and diamond grain size of samples studied here is shown in Table 1. In case of nanodiamond/pyrocarbon composites (NDC type) with 5 nm particles the sp^2/sp^3 ratio is varied from zero (diamond compact) to 0.5, thus the fraction of sp^2-bonded carbon is in the range of 0 to 33 wt%. The sample density increases from 0.85 to 2.1 g/cm^3 [39], while resistivity decreases from 10^7 to 0.1 Ωcm with sp^2 fraction. The samples with bigger grains (DPC type) were prepared with fixed sp^2/sp^3 ratio of 0.2. The samples were produced in the form of disks of 20 mm in diameter and 1 mm in thickness, however larger composite sheets, up to 100 mm diameter, can also be synthesized.

MicroRaman spectra were taken for qualitative phase analysis of the composites using "Jobin-Yvon S-3000" spectrometer. The scattering was excited at 514.5 nm wavelength of an Ar^+-ion laser focused into a 2 μm diameter spot. Field electron emission properties (I-V characteristics) were studied using a microprobe device with tungsten tip of ca. 20 μm radius placed at 10-100 μm above the sample surface [8,10]. The emission has been measured in vacuum 10^{-7} Torr at least at four different locations on each sample. A flat 30x30 mm^2 fluorescent screen was used to monitor the distribution of emission sites on the whole sample area, the images being captured by a CCD camera, and simultaneously I–V curves were recorded. A 200 μm thick glass spacer was used to fix the distance between the screen and the sample. A high D.C. voltage up to 8 kV was cyclically applied between sample and anode (microprobes or fluorescent screen), and the emission current in a range of 10 pA - 1 mA was measured. A Scanning Tunneling-Field Emission Microscope (STFEM) [8,20-22] was applied for high resolution mapping of surface topography, field electron emission intensity, surface potential (effective work function) and electrical conductivity of the samples.

3. Results

3.1. Structure characterization

Figure 2 shows Raman spectra of a nanodiamond composite (NDC) with 5 nm diamond particles and a diamond/pyrocarbon composite (DPC-1) with 0.02-1 μm diamond particles. These two samples have the same sp^2/sp^3 ratio of 0.2 but exhibit different spectra. The coarse-grained DPC-1 composite (see upper spectrum) displays the sharp diamond peak at 1329 cm^{-1} and two broad bands at 1353 cm^{-1} (D peak) and 1595 cm^{-1} (G peak) ascribed to nanocrystalline graphite. The typical size of graphite crystallites (length of basal plane) is 4 nm as evaluated from ratio of integral intensities of the D- and G-peaks: I_D/I_G=1.10 [40]. The shift of the G-band of graphite from 1580 to 1595 cm^{-1} evidences a highly disordered structure of sp^2-bonded carbon. The shift of the diamond peak from 1332 cm^{-1} known for diamond to 1329 cm^{-1} can be associated with thermal heating of isolated crystallites by laser beam, similar to that observed for highly graphitized CVD diamond films [19], evidencing that the diamond particles are completely surrounded by graphitic matrix and don't contact with each other. These observations are consistent with as-designed model of the composites where 0.1-1 μm diamond particles are surrounded with the sp^2-bonded carbon cover of about 2-10 nm thickness.

The spectrum of NDC sample displays only two bands centered at 1330 cm^{-1} and 1596 cm^{-1}, with I_D/I_G ratio of about 1.65, that belong to disordered graphite with average particle size of about 2.6 nm. XRD study showed an average size of pyrocarbon crystallites of about 1.2 and 2.4 nm for NDC-20 and DPC-1 samples, respectively [34]. However, effective thickness of the pyrocarbon shell covering the diamond particles for NDC-20 sample is about 0.4 nm as calculated from sp^2/sp^3 mass ratio. This leads to assumption that thin pyrocarbon shells look like continuous graphene or onion fragments. High-resolution TEM study directly showed separate diamond particles covered with a graphitic shell and some fragments of onion-like carbon surrounding diamond particles were indeed observed for NDC-type composites [39], that is similar to those found for nanodiamond powders during high-temperature annealing [41].

An X-ray diffraction analysis revealed the presence of diamond phase in NDC samples [42], however the diamond peak is not seen in the Raman spectrum because of (i) a broadening of the diamond peak due to phonon confinement effect in ultrafine particles [43], and (ii) much smaller scattering cross-section of diamond compared to graphite. XAES and XPS study of the composites showed [37] that a few monolayers of nanostructured sp^2 carbon remain on the surface even after hydrogen plasma treatment, while a mixture of sp^2- and sp^3- bonded carbon was observed in deeper layers.

Table 1. Composite samples studied in the present work.

Type	Diamond particle size, nm	sp^2/sp^3, wt ratio
NDC	4-6	0-0.5
DPC-0.1	10-100	0.2
DPC-1	20-1000	0.2
DPC-4	3000-5000	0.2

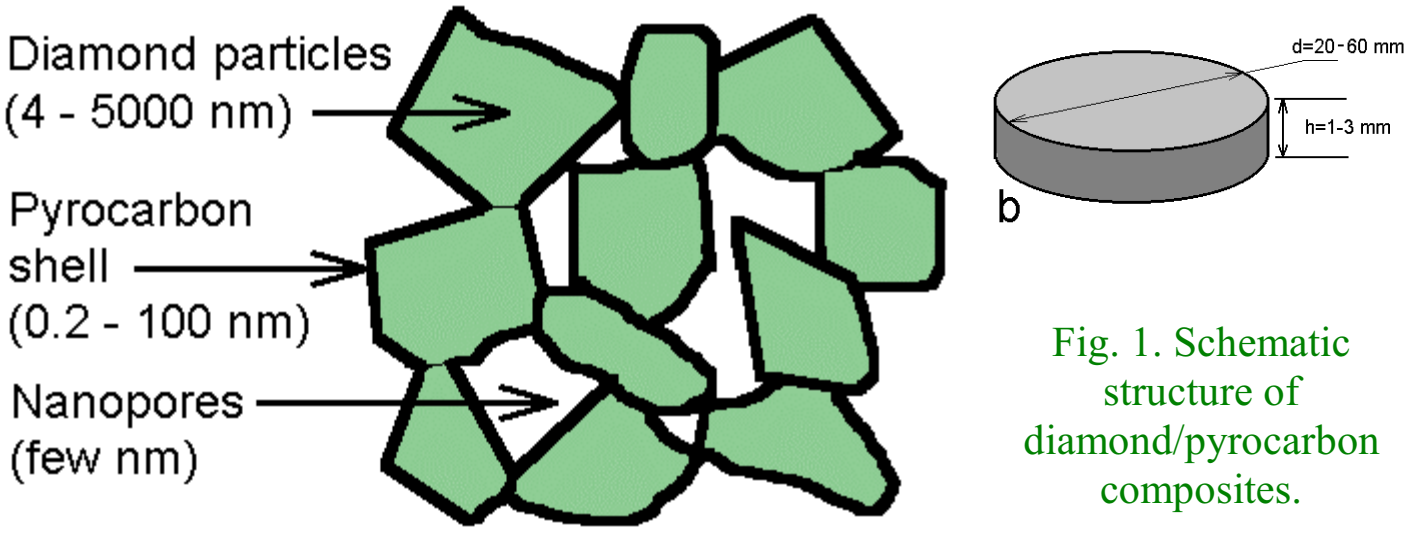

Fig. 1. Schematic structure of diamond/pyrocarbon composites.

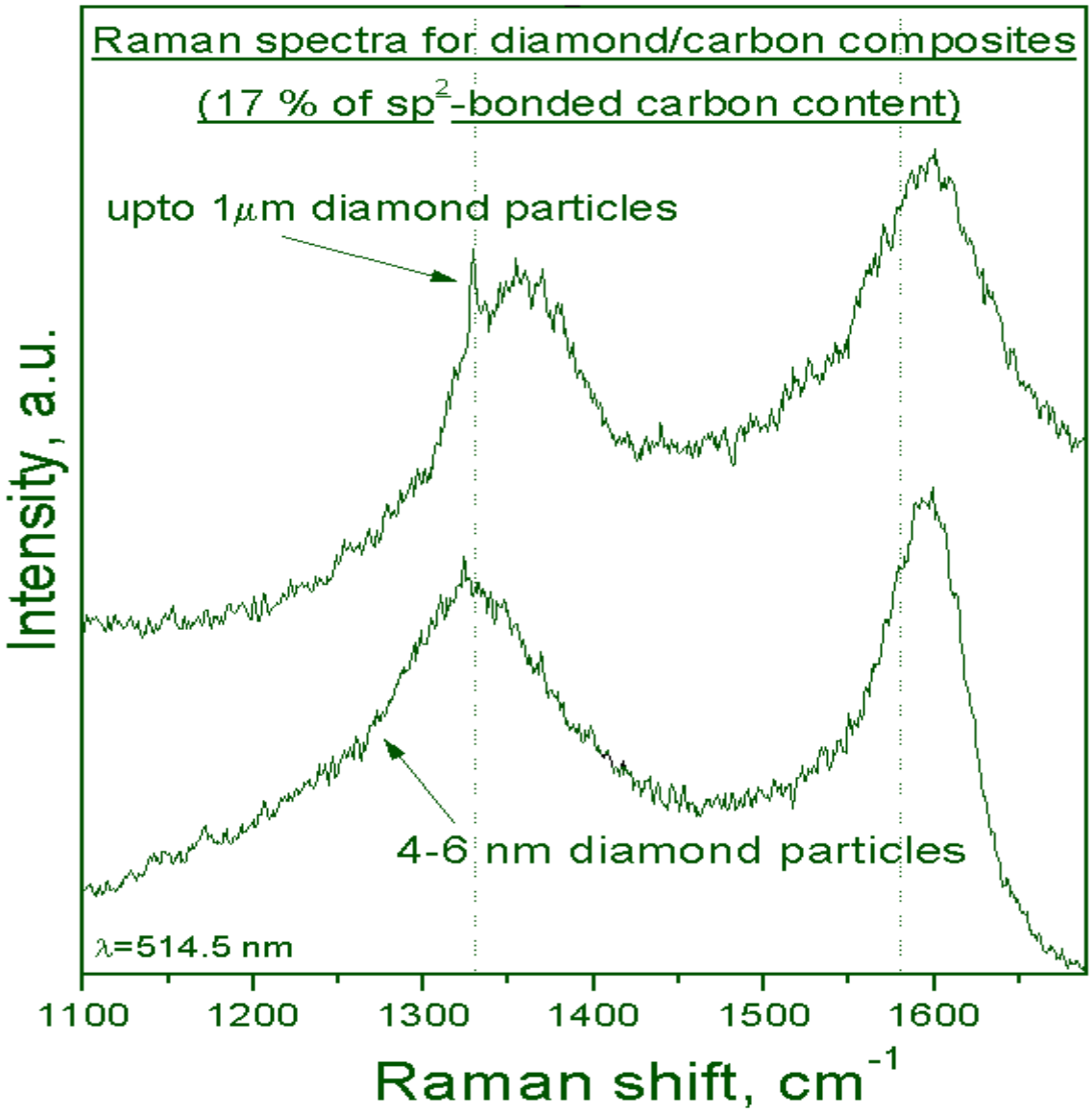

Fig. 2. Raman spectra of a nanocomposite (NDC) with 5 nm diamond particles and a DPC-1 composite with 0.1-1 μm diamond particles. Samples have the same sp^2/sp^3 ratio of 0.2.

3.2. Macroscopic field emission properties

The field electron emission strongly depends on the composite structure. Figure 3 illustrates how the emission threshold field E_{th} measured with the microprobe correlates with sp^2-bonded carbon content in the nanocomposite. The value of E_{th} is defined as the field inducing the current of 0.1 nA that corresponds to the current density of about 10 $\mu A/cm^2$. The lowest threshold of 23 V/μm is achieved at optimum sp^2 content of 15-25 wt% that is equivalent to effective (average) thickness of 0.4 -0.6 nm of the graphitic layer around 5 nm diamond particles. At higher sp^2 contents (thicker graphite layer) the emission threshold increases up to 40 V/μm. On the other hand, a depletion of the composite with the graphite leads to a dramatic increase in E_{th}, its value being as high as 200 V/μm for graphite-free nanodiamond compact.

The dependence of the emission threshold on diamond particle size in the composites is shown in Fig. 4. The sp^2 carbon content for these composites was close to optimum value of 17 wt%. The I-V curves were measured with the microprobe and fluorescent screen (in the latter case the threshold field refers to 1 nA current from ~2 cm^2 emission area). The microprobe data for each sample were obtained in several sites, and then the results were averaged. Thus determined thresho ld fields were systematically higher by a factor of 3-7, than E_{th} values measured by the screen technique. This can be explained by an effect of surface inhomogeneities and statistical distribution factors. A small number of sites with very low threshold m ay present on the large area monitored with the screen. Fluctuations in structure and relief (single high protrusions), as well as contaminations, may cause the emission onset at reduced fields. In contrast, the microprobe data being averaged provide "true" emission characteristic of the material, especially in case when the screening shows only rare emitting sites. Yet, for both measurement techniques an optimum structure of the composite that provides the lowest E_{th} is achieved with diamond particle size of 10-100 nm. This corresponds to thickness of surrounding graphitic layer of 0.4 -4 nm. The use of ultradispersed diamond particles of ~5 nm, and large diamond grains of 3 -5 μm leads to poorer surface uniformity of the emission (small number of emission sites as shown by arrows in Fig. 4) and higher emission threshold fields.

Fig. 5 shows I-V curves for one of the best composite with 100 nm diamond grains (DPC-0.1 sample, sp^2/sp^3 =0.2). The emission begins at fields of 1.1 V/μm, and well fits the Fowler-Nordheim plot (Fig. 5, inset). There are no hysteresis or activation processes during many cyclings of the applied voltage. The current of 1 mA through ~2 cm^2 screen area can be easily achieved and reproduced. The surface distribution of the emission sites as seen with the fluorescent screen (Fig. 6) looks more or less uniform, yet a higher density of emitting sites may be required for technical applications. The density of the emission sites for the best samples is about of 5 x 10^2 cm^{-2}, while a map of the sites was stable at voltage cycling during at least 8 hours.

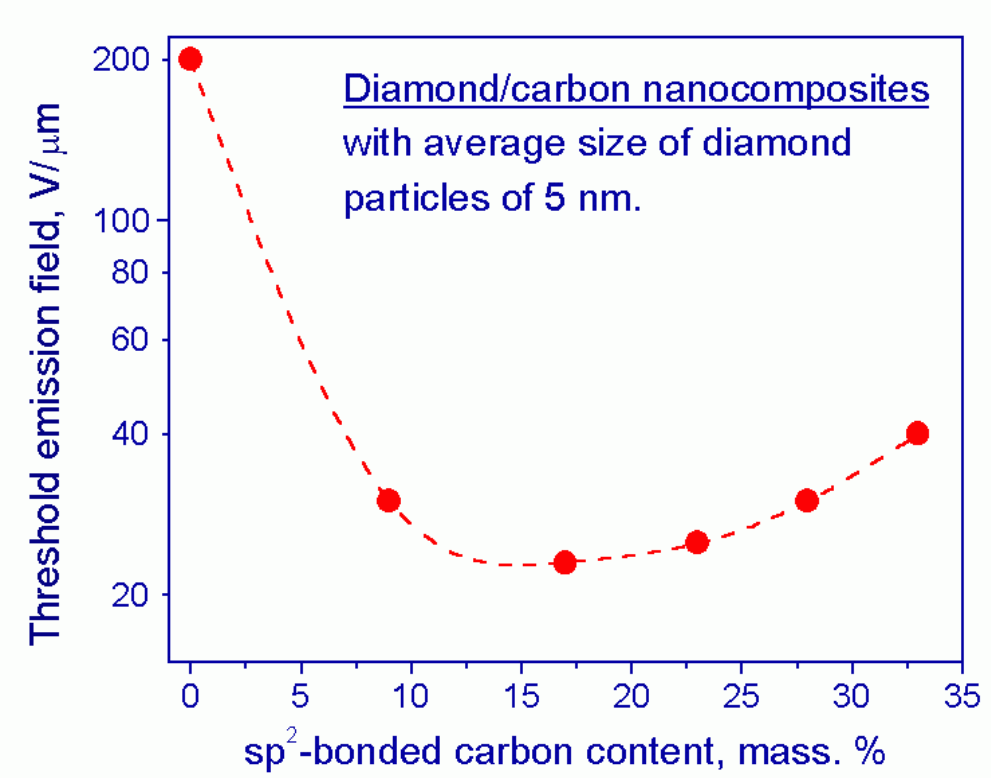

Fig. 3. Emission threshold field E_{th} vs sp^2-bonded carbon content in the NDC-type nanocomposites. The effective thickness of sp^2-bonded carbon shell around the diamond particles is changed from zero (left point) to 1 nm (right one). The best emission corresponds to effective shell thickness of 0.4-0.6 nm.

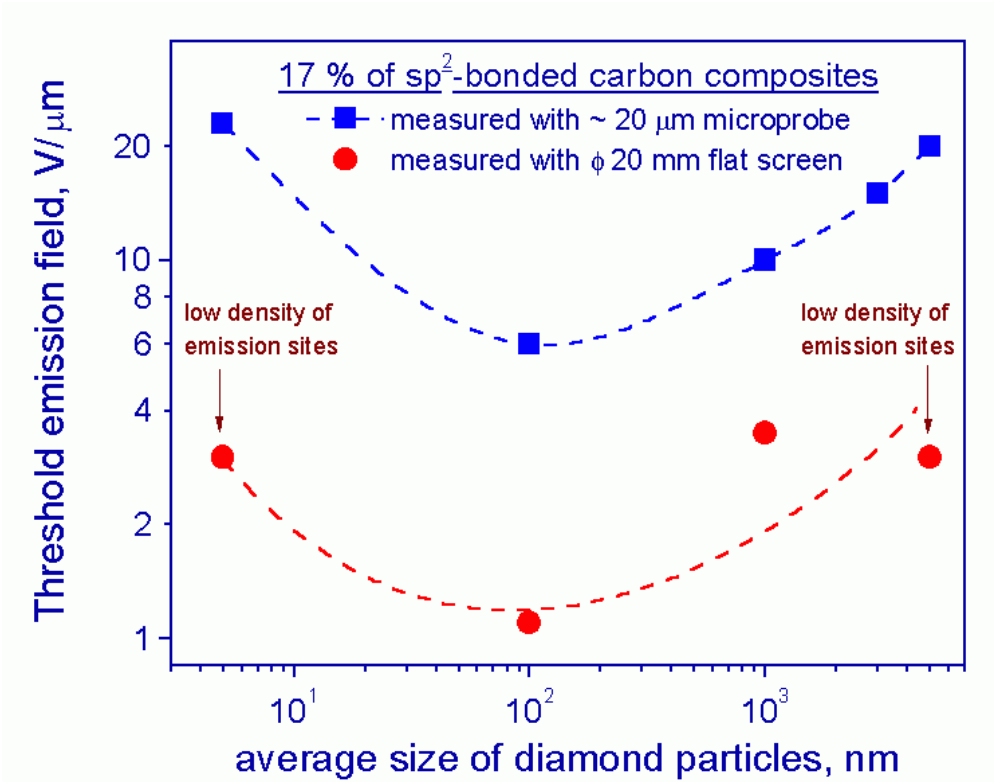

Fig. 4. Emission threshold field versus diamond particle size in composites with sp^2/sp^3=0.2 as measured with tungsten microprobe (squares) and fluorescent screen (circles). The onset of emission at field as low as 1 V/μm is observed with the screen for the sample DPC-0.1 with 10-100 nm diamond particles. The best emission corresponds to effective shell thickness of about 0.4-4 nm.

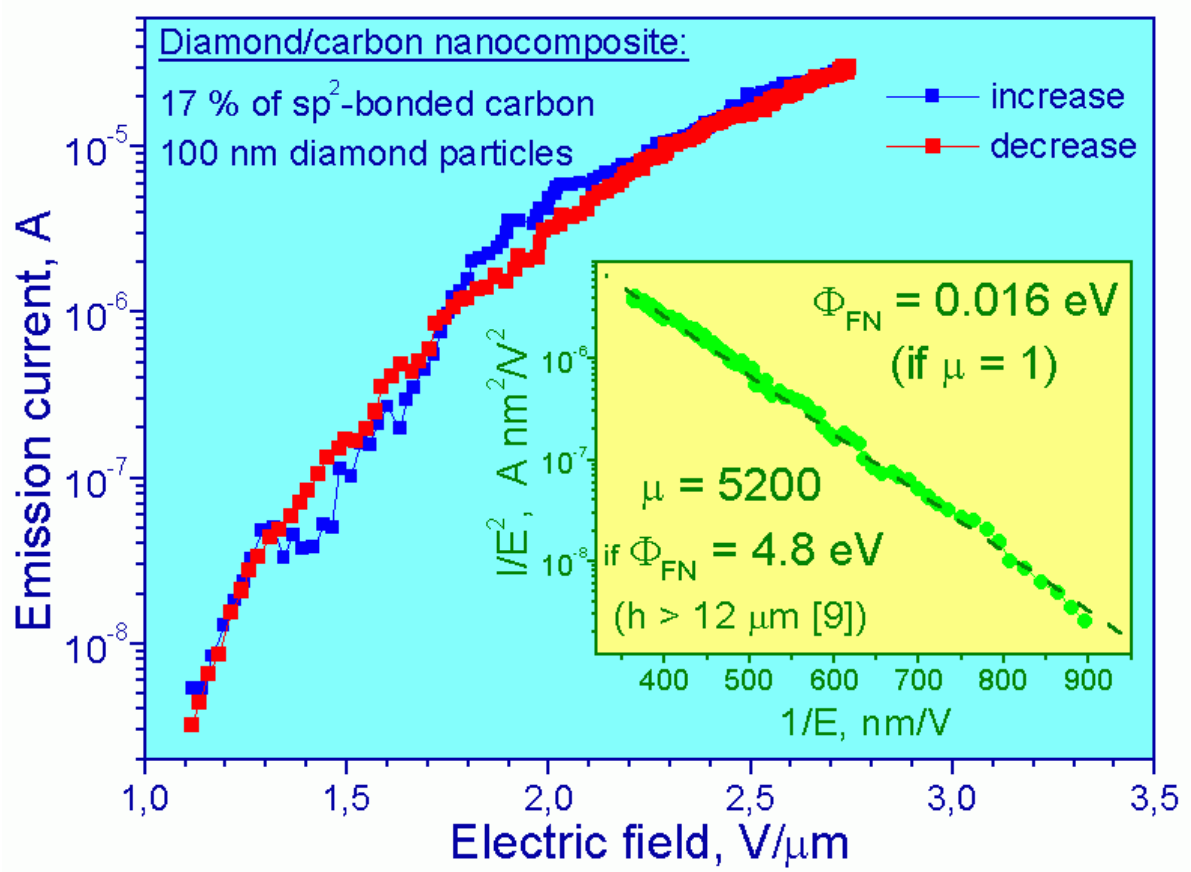

Fig. 5. I-V curves for the DPC-0.1 composite recorded at increasing field (open squares) and decreasing field (closed squares). Fowler-Nordheim plot is shown in inset.

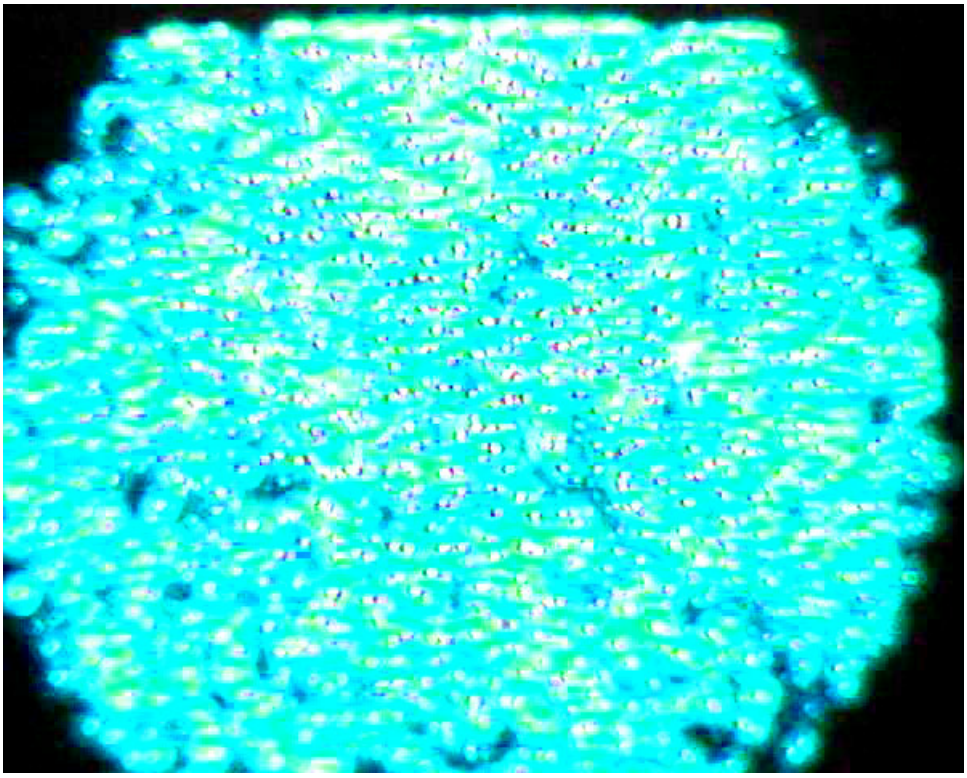

Fig. 6. The distribution of emission sites for one of the best DPC sample visualized wit h fluorescent screen. Diameter of the emitting area is 20 mm, cathode current of 800 μA at field of 10 V/μm.

3.3. Microscopic emission study

To understand the nature of the emission sites the high-resolution emission mapping with STFEM was applied. Figure 7 shows typical maps of topography, field emission intensity, electrical conductivity and surface potential for the DPC-0.1 sample taken at the same 1.5x1.5 μm^2 area. The emission zones are clearly bounded to some hillocks (grains) of about 0.5-1 μm in diameter and height (compare Fig. 7 a,b). Note that these grains are formed (agglomerated) as a rule from a number of smaller diamond particles [44], and have no sharp tip-like protrusions. Moreover, the electrical conductivity on the top of the emitting grains demonstrates relatively low ("non-graphite") values, not like for an insulator (diamond), but rather typical for a semiconductor or a thin (2D) conducting (graphitic) layer (Fig. 7c). The effective work function (surface potential) is also lower in these emitting zones compared to the background (Fig. 7d). Unfortunately, it is difficult to quantify the conductivity and the work function scales; therefore they are given here in arbitrary units.

We ascribe the emission region to aggregated diamond grains, most probably with thin graphite coverage, at least much thinner than on surrounding surface area. The uncovered diamond phase sometimes appears on the sample surface that can be concluded from conductivity maps measured with the STFEM, in such case the emission spots are revealed near the border of these areas. But, as a rule, the graphite forming well-conducting surface regions on the grains covers the diamond. Similar observation was previously reported for nanocomposites prepared with 5 nm diamond particles [37] where local emission maxima coincided with the tops of the surface protrusions (grains), while the effective work function often was minimal at those sites.

Metodics: Specially designed high vacuum STFEM device gives 4 maps simultaneously

1) Morphology of the surface,
2) Local field electron emission intensity,
3) Distribution of surface potential barrier for emitted electrons (local work function),
4) Local surface electrical conductivity evaluation.

- uses tunneling and field emission regimes;
- apply to semisonducting and semi-insulation films;
- upto 12x12 μm^2 maps inside a square of 5x5 mm^2 in vacuum

$1/E(I_o) = \Delta Z/\Delta U$ – field electron emission intensity signal;
$\Phi^{3/2} = C\,(U/I_o)\,(\Delta I/\Delta Z)$ – effective work function signal;
$\rho \sim \Delta I/\Delta Z$ – electrical conductivity evaluation signal.

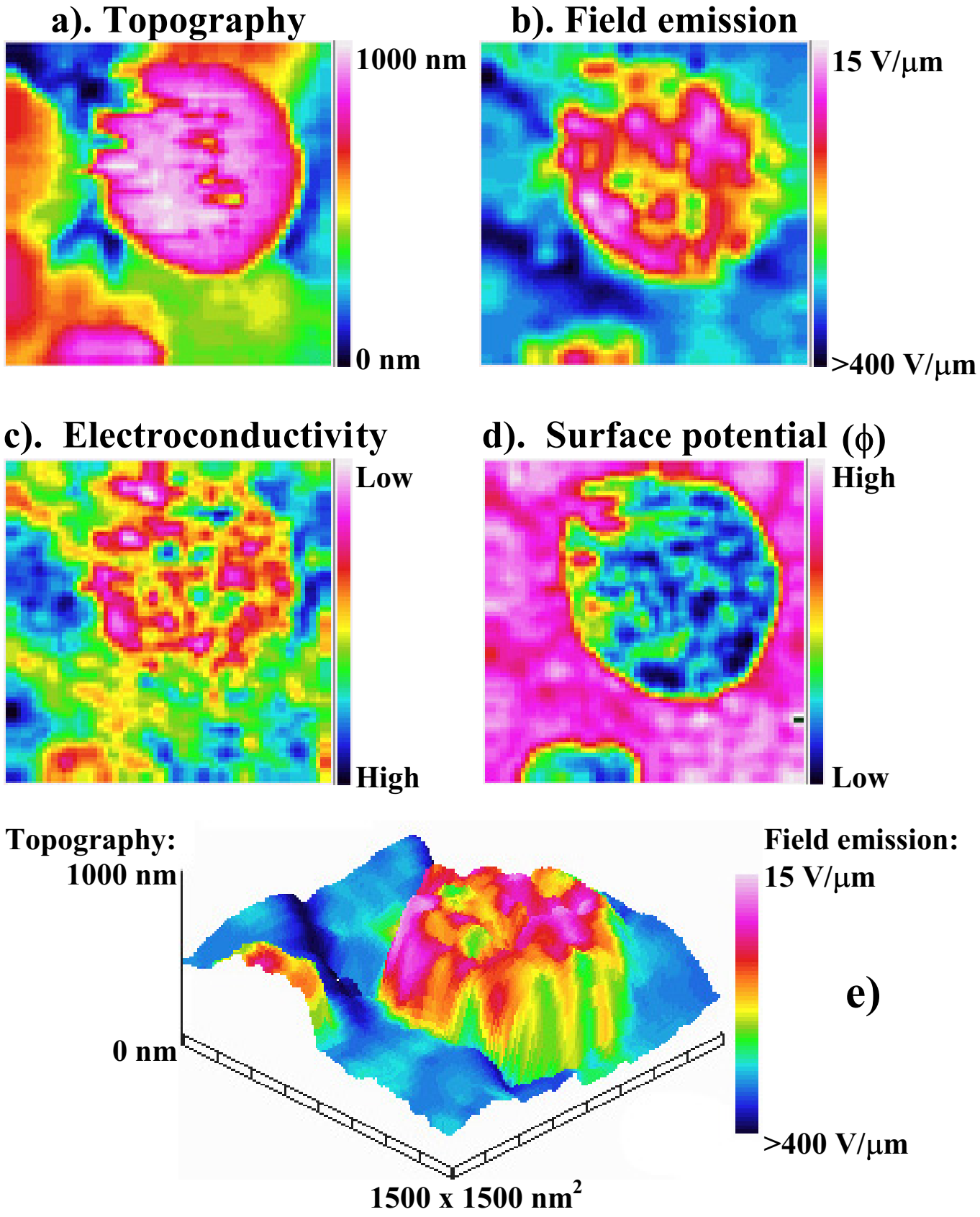

Fig. 7. 2D mapping of topography (a), field emission (b), electrical conductivity (c) and surface potential (d) measured with STFEM for DPC-0.1 sample. (e) 3D topography arranged with color (gray-scale brightness) emission map. Sampling area: 1.5x1.5 μm².

4. Discussion

There is a certain analogy in structure of the diamond/pyrocarbon composites examined here and CVD diamond films containing the graphitic phase in significant amounts, and showing the electron emission at low (a few V/μm) fields [17,19]. This similarity is depicted schematically in Fig. 8. The graphite-like phase is located at grain boundaries in those nanocrystalline films, and the emission has been found to origin mostly from the grain boundaries and diamond/graphite interfaces [19-22]. Below we briefly consider the emission mechanisms that take into account the coexistence two carbon phases, and that could be applicable for the composites as well as for the diamond films.

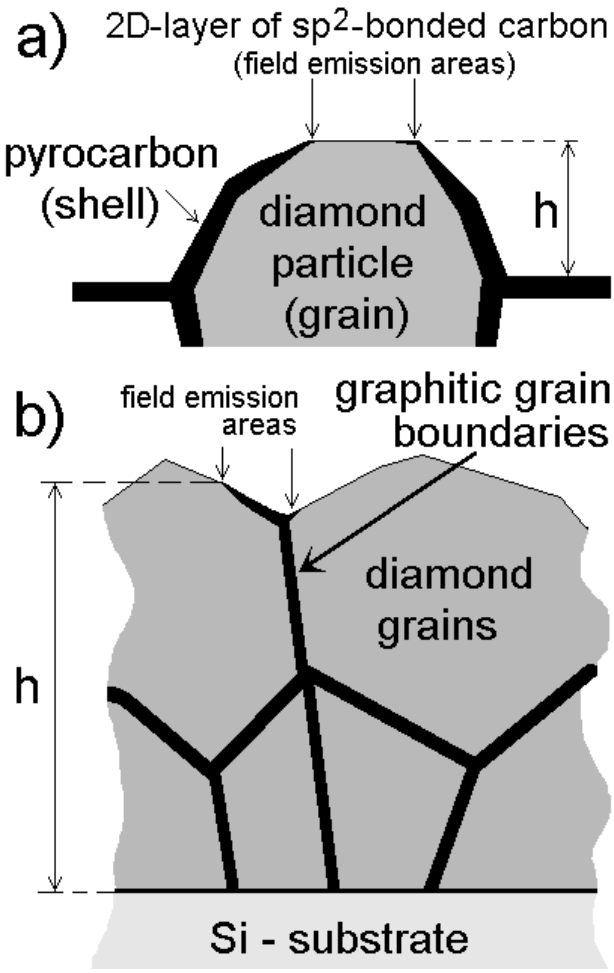

Fig. 8. The schematic surface structure of the diamond/carbon composite (a) and CVD diamond film containing the graphitic phase at grain boundaries (b). The outer surface may expose uncovered diamond as well as thin or thick graphite layers on diamond particle.

4.1. Compromise between field enhancement and low barrier

Low-field emission from carbon materials sometimes is ascribed just to local field amplification by protrusions or columnar grain boundaries with high aspect ratio [17,26,45]. Typically the field enhancement factor μ of the order of 1000 and even higher is required to explain the experimental data. Since there are no such high and sharp tips on the composite surface, or long enough narrow conducting channels in the insulating diamond matrix in thin (<1 μm) CVD film, the emission hardly can be ascribed to the geometric field enhancement only. Indeed, the effective work function derived from the Fowler-Nordheim plot (Fig. 5, insert) is improbably low Φ=0.016 eV in the case of zero field enhancement (μ=1). Assuming the work function to be of graphite Φ=4.8 eV the field enhancement must be very large (μ=5200). It can be estimated that in order to provide so high enhancement factor, an atomically sharp tip must have the height of more than 10 μm (because in this case the tunneling barrier is not triangle, but logarithmic, see [20] for details). Such high protrusions were not observed on these samples. Hence, an essential reduction of the surface tunneling barrier height should be suggested.

On the other hand, the barrier cannot be as low as 0.015-0.3 eV (comparing with 0.03 eV of kT at room conditions), otherwise thermionic emission would be observed at room temperature [46]. So a combination of local field enhancement and low work function most probably takes place [20].

4.2. Low tunneling barrier for diamond/graphite surfaces

A decrease of the tunneling barrier for escaping electrons can be caused, for example, by covering the diamond with an ultrathin conducting layer, e.g. metals as found by different authors [5,8,30-32,47,48], that leads to a negative surface band bending. T he negative electron affinity of "uncoated" diamond [28-33] also can play an important role. The possible ways of tunneling process are shown schematically for the composite and a diamond film in Fig. 9. Near the diamond/graphite interface two cases can be considered.

The first mechanism implies the emission from diamond surface covered by an ultrathin graphitic layer transparent for tunneling (Fig. 9a). Electrons are injected from graphite to diamond and then emitted as "diamond electrons" through the barr ier, lowered due to NEA or band bending. In this case the presence of NEA for the graphite-coated diamond is assumed, like that for some metal coatings [5,30-32]. So the emission area is located on outer graphitic surface near diamond/graphite interface and is determined, in particular, by local thickness of conducting (graphitic) layer.

The second possibility is the emission from NEA diamond surface (exposed to vacuum), where electrons are injected from graphite to diamond [3,5,15-17,22], then diffuse to the diamond surface (Fig. 9b). In this case the emission area is located on diamond surface near diamond/graphite interface and limited by carrier diffusion length in diamond [22].

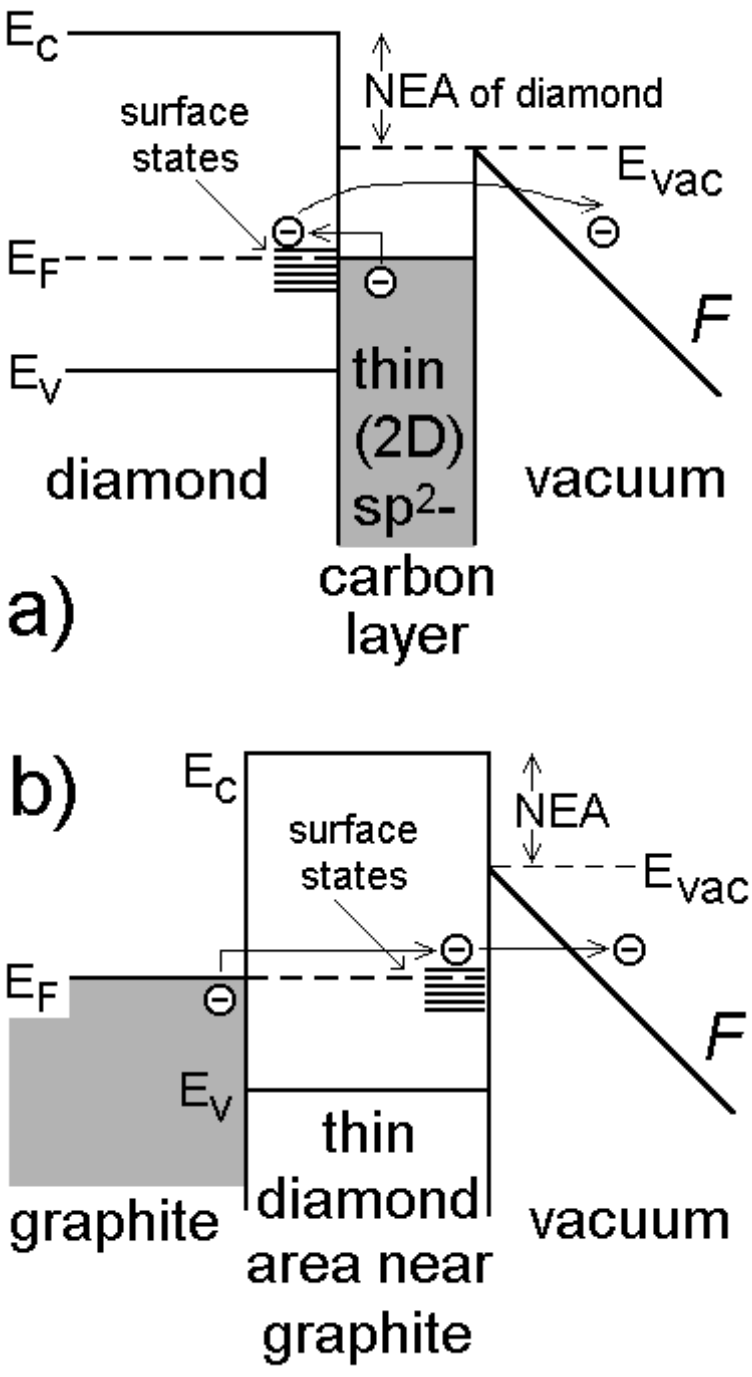

Fig. 9. Two possible processes of electron tunneling in the composite or diamond film. (a) Emission from diamond surface covered with thin graphitic layer. Electrons are injected from graphite to diamond and then emit as "diamond electrons" through the barrier, lowered due to NEA or band bending. (b) Electrons are injected through graphite/diamond interface (like "back-contact"), and then diffuse to the diamond surface with low or NEA.

As noted in section 4.1, the effects of the field enhancement and lowered work function should be combined to explain the low emission thresholds observed. Nevertheless, such the explanation is problematic even in the case when the Fermi level is placed near the middle of the diamond bandgap. Indeed, if we assume the position of the Fermi level E_F above the valence band maximum E_v to be E_F-E_v=1.4 eV for diamond (as reported for diamond/graphite Schottky barrier [33]), and the value of NEA as deep as -2.05 eV [33], the tunneling barrier height will be about φ=2.0 eV (Fig. 9a).

This means, that for the emission threshold field of 1 V/ μm (Fig. 5) the height of atomically sharp protrusion (or the length of single grain boundary) must be more than 6 μm (see [20] for detailed calculation). This seems to be unrealistic for the diamond/pyrocarbon composites studied here as well as for thin CVD diamond/ graphite films [19-22], because such high and sharp protrusions were not found in our STFEM and SEM studies, and the length of a grain boundary can not be longer the film thickness (~ 1 μm) or diamond crystallite size (less than 100 nm for the composite sh own in Fig.5).

Thus, even in the case of realistically low tunneling barrier for diamond it is hardly to find necessary field enhancement for these samples, and such the models using diamond properties have a limited application for the low-field electron emission observed.

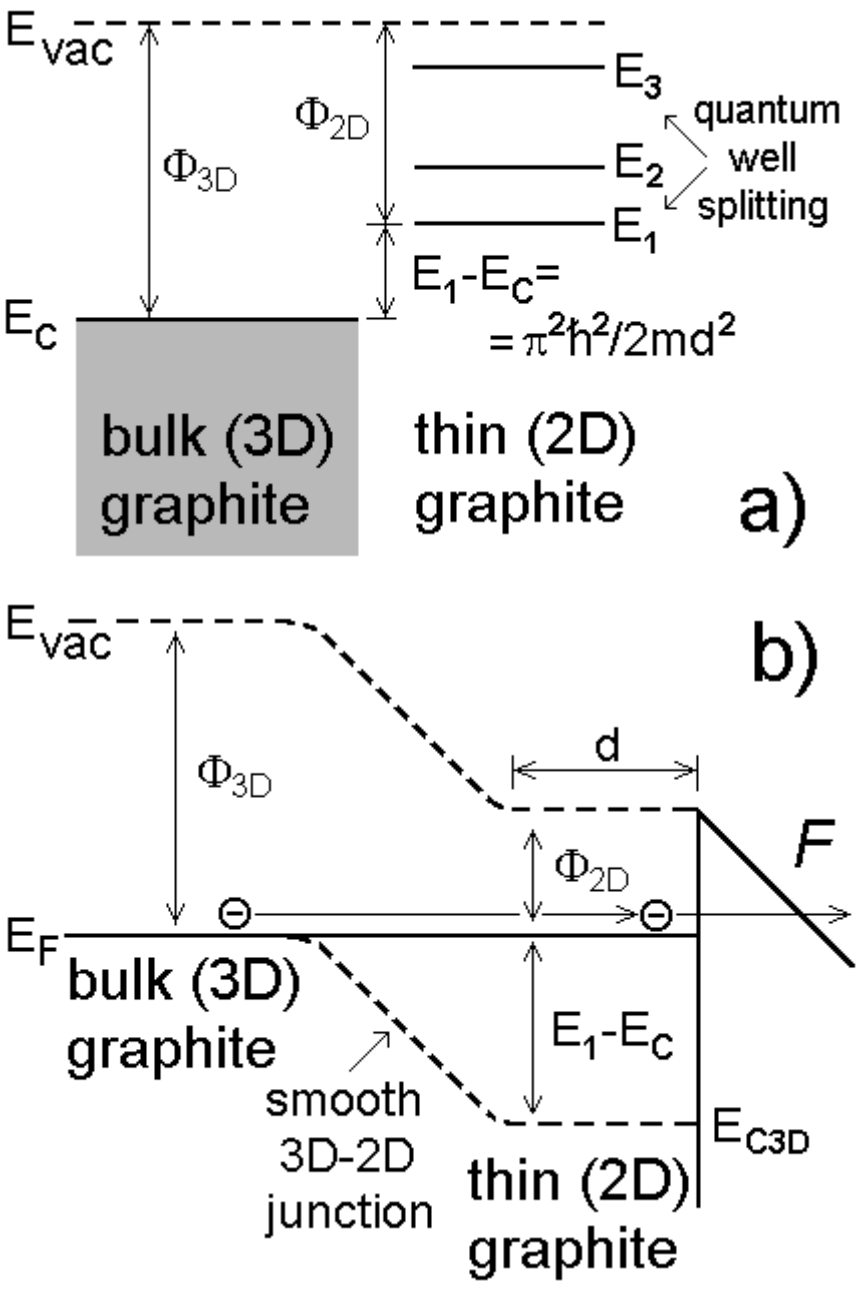

Fig. 10. The quantum well splitting of conduction band of a thin 2D graphite layer adjacent to bulk graphite (a), and the band diagram of low barrier emission for smooth 3D/2D junction of graphite (b).

4.3. Emission from graphitic quantum well

One more emission mechanism takes into account a quantum well effect in thin two-dimensional (2D) graphitic layer covering the insulating diamond grains or located between the grains. The quantum well splitting of the conduction band of a thin 2D graphite layer is shown schematically in Fig. 10a. The distance between the first subband of 2D well and the bulk conduction band of graphite, E_1-E_C, depends on thickness of graphite layer, d, as E_1-E_C=$h^2/8md^2$, where h is Plank constant, m - effective electron mass. The value E_1-E_C increases with d decrease, that facilitates the electron emission, since the work function of 2D-layer could be lower than of bulk graphite. The band diagram for smooth 3D/2D junction of graphite (appearing, for example, on edge of graphite coating of diamond particle, see Fig. 8) shows that the tunneling barrier for electrons can be reduced to ~1 eV for the layer thickness of about 0.6 nm (Fig. 10b). Such the effective graphite layer thickness is quite typical for the diamond/pyrocarbon composites studied here and often corresponds to the best emission properties (see section 3.2). Moreover, an increasing as well as a decreasing of the effective pyrocarbon thickness from this optimum value leads to deterioration of the emission properties (Fig. 3,4).

Another way to evaluate the effect of 2D-layer on the emission (particularly in the case when upper 2D-subbands are populated) was described in Ref. [22] using electron state density of 2D layer and surface carrier concentration. Besides, fine (thin) graphite structures can show unique electronic properties. For example, schwarzites, onion-like clusters, and nanotubes can be both narrow band gap semiconductors, and dielectric or semimetal [49,50]. Moreover, preliminary calculations made by Chernozatonsky [51] showed that the work function on the edge of graphene (single basal plane of graphite) could be as low as 1 eV. We note, that the onion-like fragments as well as nanosized regions with semiconducting-like electrical conductivity were observed in these diamond/pyrocarbon composites during TEM [39] and STFEM (section 3.3) studies.

Using the value of the work function φ~1 eV it is possible to describe the low-field emission from the nanocomposites studied using a realistic value of the field enhancement. We emphasize, that the quantum well model does not require a presence of specific diamond properties (NEA) and can be applied to a wide range of carbon materials. Does the diamond really play the unique role in the considered process of emission, we have doubt.

Summarizing, the low-field electron emission mechanisms for the diamond/carbon composites unlikely can be ascribed solely to specific diamond properties, while the presence of nanostructured sp^2-bonded carbon probably is of key importance. Nevertheless, a presence of the diamond phase is desirable to provide the best emission properties achieved due to better thermal conductivity [39] and promoting for fine graphite structure formation. Essentially, that although the local structure of the sp^2-bonded carbon matrix in the composite may be similar to that of pyrolytically produced bulk glassy carbon, the former exhibits superior emission properties (threshold fields are in the range of 30-100 V/μm for glassy carbon [18]) presumably due to the 2D nature of graphite shell around diamond. Thus, a role of graphite in the suggested low-field electron emission mechanism is by no means simply in providing the electrical conductivity of the sample, rather the fine nanostructure of the diamond/graphite interfaces and the sp^2-bonded carbon phase becomes important.

4. Conclusions

1. Perspective class of carbon materials - diamond/pyrocarbon nanocomposites - was designed and studied for the field electron emission in dependence of their structure.

2. The emission at fields of as low as 1 V/μm was reproducibly obtained with good surface uniformity.

3. The microstructural analysis and the Scanning Tunneling-Field Emission Microscopy show the preferable emission from semiconducting-like low-work-function regions that could be ascribed to ultrathin (two-dimensional) pyrocarbon coverage of the diamond particles.

4. Three models of the low-field emission using the thin graphite layer on the diamond were analyzed. It was shown, that two of them that relay on specific diamond properties (NEA) couldn't explain low emission thresholds at realistic value of the field enhancement.

5. The quantum well model was suggested to explain the low-field emission from the nanocomposites using electronic properties of 2D conducting layers of sp^2-bonded carbon on dielectric diamond particles. It was concluded, that the emission mechanism for the nanocomposites unlikely could be ascribed to unique diamond properties, whereas the sp^2-bonded nanocarbon phase probably plays a key role.

Acknowledgements The authors are grateful to Skeleton Technologies Group for the financial support of the studies, to Dr. V. D. Frolov for discussion of the emission mechanisms and Dr. I. I. Vlasov for the Raman spectroscopy.

REFERENCES

[1] C. Wang, A. Garcia, D. C. Ingram, M. Lake, and M. E. Kordesch, Electron. Lett. 27, 1459 (1991).
[2] M. W. Geis, N. N. Efremov, J. D. Woodhouse, M. D. McAleese, M. Marchywka, D. G. Socker, and J. F. Hochedez, IEEE Electron Device Lett. 12, 456 (1991).
[3] N. S. Xu, Y. Tzeng, and R. V. Latham, J. Phys. D.: Appl. Phys. 27, 1988 (1994).
[4] J. D. Shovlin and M. E. Kordesch, Appl. Phys. Lett. 65, 863 (1994).
[5] M. W. Geis, J. C. Twichell, J. Macaulay, and K. Okano, Appl. Phys. Lett. 67, 1328 (1995).
[6] W. Zhu, G. P. Kochalski, S. Jin, L. Seibles, D. C. Jacobson, M. McCormack, and A. E. White, Appl. Phys. Lett. 67, 1157 (1995).
[7] K. Okano, K. Koizumi, S. R. P. Silva, and G. A. J. Amaratunga, Nature 381, 140 (1996).
[8] A. V. Karabutov, V. I. Konov, S. M. Pimenov, V. D. Frolov, E. D. Obraztsova, V. I. Polyakov, and N. M. Rossukanyi, J. de Phys. IV C5, 113 (1996).
[9] G. A. J. Amaratunga and S. R. P.Silva, Appl. Phys. Lett. 68, 2529 (1996).
[10] A. V. Karabutov, V. I. Konov, V. G. Ralchenko, E. D. Obraztsova, V. D. Frolov, S. A. Uglov, M. S. Nunuparov, H.-J. Scheibe, V. E. Strelnitskij, V. I. Polyakov, and N. M. Rossukanyi, J. CVD 5, 348 (1997).
[11] B. S. Satyanarayana, A. Hart, W. I. Mline, and J. Robertson, Appl. Phys. Lett. 71, 1430 (1997).
[12] A. G. Rinzler, J. H. Hafner, P. Nikolaev, L. Lou, S. G. Kim, D. Tomanek, P. Nordlander, D. T. Colbert, and R. E. Smalley, Science 269, 1550 (1995).
[13] W. A. de Heer, A. Chatelain, and D. Ugarte, Science 270, 1179 (1995).
[14] I. Musa, D. A. I. Munindrasdasa, G. A. J. Amaratunga, and W. Eccleston, Nature 395, 362 (1998).
[15] S. Jou, H. J. Doerr, and R. F. Bunshah, Thin Solid Films 280, 256 (1996).
[16] A. A. Talin, L. S. Pan, K. F. McCarty, T. E. Felter, H. J. Doerr, and R. F. Bunshah, Appl. Phys. Lett. 69, 3842 (1996).
[17] F. Lacher, C. Wild, D. Behr, and P. Koidl, Diamond Relat. Mater. 6, 1111 (1997).
[18] S. M. Pimenov, E. N. Loubnin, E. D. Obraztsova, A. V. Karabutov, V. V. Kononenko, and V. I. Konov, Proc. Int. Symp. on Diamond Materials V, Electrochemical Soc, vol. 97-32, 537 (1998).
[19] A. V. Karabutov, V. I. Konov, S. M. Pimenov, E. D. Obraztsova, V. D. Frolov, V. G. Pereverzev, and A. A. Smolin, Journal of Wide Bandgap Materials 7, 68 (1999).
[20] A. V. Karabutov, V. D. Frolov, S. M. Pimenov, and V. I. Konov, Diamond Relat. Mater. 8, 763 (1999).
[21] V. D. Frolov, A. V. Karabutov, V. I. Konov, S. M. Pimeniov, and A. M. Prokhorov, J. Phys. D: Appl. Phys. 32, 815 (1999).
[22] V. D. Frolov, A. V. Karabutov, S. M. Pimeniov, E. D. Obraztsova, and V. I. Konov, Ultramicroscopy 79, 209 (1999).
[23] A. T. Rakhimov, N. V. Suetin, E. S. Soldatov, M. A. Timofeyev, A. S. Trifonov, and V. V. Khanin, Proc. of the 11th IVMC, 19-24 July 1998, Asheville, USA, p. 224.
[24] V. D. Frolov, A. V. Karabutov, S. M. Pimeniov, and V. I. Konov, Diamond Relat. Mater. 9, 1196 (2000).
[25] Y. D. Kim, W. Choi, H. Wakimoto, S. Usami, H. Tomokage, and T.Ando, Diamond Relat. Mater. 9, 1096 (2000).
[26] O. Gröning, O. M. Küttel, P. Gröning, and L. Schlapbach, J. Vac. Sci. Technol. B 17, 1970 (1999).
[27] A. N. Obraztsov, I. Yu. Pavlovskj, A. P. Volkov, A. S. Petrov, V. I. Petrov, E. V. Rakova, and V. V. Roddatis, Diamond Relat. Mater. 8, 814 (1999).
[28] F. J. Himpsel, J. A. Knapp, J. A. Van Vechten, and D. E. Eastman, Phys. Rev. B 20, 624 (1979).
[29] C. Bandis and B. B. Pate, Phys. Rev. Lett. 74, 777 (1995).
[30] J. van der Weide, Z. Zang, P. K. Baumann, M. G. Wensell, J. Bernholc, and R. J. Nemanich, Phys. Rev. B 50, 5803 (1994).
[31] R. J. Nemanich, P. K. Baumann, M. C. Benjamin, S. W. King, J. van der Weide, and R. F. Davis, Diamond Relat. Mater. 5, 790 (1996).
[32] P. K. Baumann and R. J. Nemanich, Diamond Relat. Mater. 7, 612 (1998).
[33] J. Robertson and M. J. Rutter, Diamond Relat. Mater. 7, 620 (1998).
[34] S. K. Gordeev, S. G. Zhukov, Yu. I. Nikitin, and V. G. Poltoratskij, Inorganic Materials 31, 470 (1995) *(in Russian).*
[35] S. K. Gordeev, S. G. Zhukov, P. I. Belobrov, A. N. Smolianinov, and Ju. P. Dikov, Russian Patent PCT Patent WO#97/11923 (03.04.1997). Russian Patent RU #2093695 (1997).
[36] S. K. Gordeev, V. G. Ralchenko, S. G. Zhukov, A. V. Karabutov, P. I. Belobrov, and M. A. Negodaev, PCT Patent WO#99/34385, (08.07.1999). Russian Patent RU #2137242 (1999).
[37] V. Ralchenko, A. Karabutov, I. Vlasov, V. Frolov, V. Konov, S. Gordeev, S. Zukov, and A. Dementjev, Diamond Relat. Mater. 8, 1496 (1999).
[38] A. V. Karabutov, V. G. Ralchenko, S. K. Gordeev, V. D. Frolov, V. I. Konov, I. I. Vlasov, and P. I. Belobrov, Paper presented at the 10th European Conf. "Diamond'99", 12-17 Sept. 1999, Prague, Chech Republic, Book of abstracts, paper 17.4.
[39] A. Vlasov, V. Ralchenko, S. Gordeev, D. Zakharov, I. Vlasov, A. Karabutov, and P. Belobrov, Diamond Relat. Mater. 9, 1104 (2000).
[40] F. Tuinstra and J. L. Koening, J. Chem. Phys. 53, 1126 (1970).
[41] V. L. Kuznetzov, A. L. Chuvilin, Yu. V. Butenko, I. Yu. Mal'kov, A. K. Gutakovskii, S. V. Stankus, and R. Kharulin, MRS Symp. Proc. 359, 105 (1995).
[42] E. N. Loubnin (unpublished).
[43] R. J. Nemanich, J. T. Glass, G. Lucovsky, and R. E. Shroder, J. Vac. Sci. Technol. A 6, 1783 (1988).
[44] P. I. Belobrov, Proc. of Fourth Internation Symposium on Diamond Films, Sept. 20-25, 1999, Kharkov, Ukraine, p. 290.
[45] V. V. Zhirnov, E. T. Givargizov, and P. S. Plekhanov, J. Vac. Sci. Technol. B 13, 418 (1995).
[46] V. V. Zhirnov and J. J. Hren, MRS Bulletin, September, 42 (1998).
[47] V. I. Polyakov, N. M. Rossukanyi, A. I. Rukovishnikov, S. M. Pimenov, A. V. Karabutov, and V. I. Konov, J. Appl. Phys. 84, 2882 (1998).
[48] P. W. May, J. C. Stone, M. N. R. Ashford, K. R. Hallman, W. N. Wang, and N. A. Fox, Diamond Relat. Mater. 7, 671 (1998).
[49] M.-Z. Huang, W. Y. Ching, and T. Lenosky, Phys. Rev. B 47, 1593 (1993).
[50] J.-C. Charlier and J.-P. Issi, Appl. Phys. A 67, 79 (1998).
[51] L. A. Chernozatonskii, private communication.